Array Pattern Control and Synthesis

R. C. HANSEN, LIFE FELLOW, IEEE

Invited Paper

Antenna array distributions and their associated patterns are now designed on physical principles, based on placement of zeros of the array polynomial. An overview of the synthesis processes is given. Robust and low Q distributions for linear arrays and circular planar arrays, that provide variable side lobe level pencil beam patterns, are treated in detail. Associated difference patterns are included. Individual side lobes or groups of side lobes may be adjusted in level. The same technique allows synthesis of an efficient shaped beam, with or without side lobe adjustment. Finally, the ultimate pencil beam array, the superdirective array, is evaluated.

I. Introduction

The control of side lobe topology in pencil beam patterns, and the synthesis of shaped beam patterns are discussed in this paper. Primary emphasis is on linear and planar broadside apertures and arrays; because of their lesser importance, endfire and ring arrays will be only briefly mentioned. Although arrays are discreet, continuous aperture distributions are commonly sampled to provide the excitations for large arrays. In a few cases, discreet distributions that are suitable for any size of array have been developed. In the 1940's aperture distributions were chosen for easy integrability, even though the results were usually difficult to use. Since modern computer power has been available, aperture distributions based on physical principles have been used. These principles for pencil beam antennas were developed primarily by Taylor [1], and are summarized as follows. Symmetric amplitude distributions are more efficient; nonsymmetric distributions produce symmetric patterns but are less efficient. Array polynomial zeros should be real; zeros off the unit circle raise side lobe nulls and side lobe heights. A $1/u$ envelope provides a robust, low Q distribution. Pattern zeros for wide angles should be separated by unity in the normalized variable $u = (d/\lambda)$ sin θ, where θ is from broadside.

Pencil beam antennas are frequently specified by the level of the first side lobe; it is convenient to use the inverse of this level, which is called side lobe ratio (SLR). The distributions to be discussed are all based on the proper adjustment of pattern function zeros to produce an efficient and appropriate pattern. Distributions of limited utility include Gaussian, cosine-on-a-pedestal, and others that involve two or more parameters. The truncated Gaussian is of course in this category. Two-parameter distributions are usually difficult to optimize, and their zero placement, hence efficiency, is almost always nonoptimum.

Manuscript received September 10, 1990; revised February 15, 1991.
The author is with R. C. Hansen, Inc., Tarzana, CA 91357.
IEEE Log Number 9105091.

II. A Pencil Beam From a Linear Array

Distributions discussed in this section are Dolph–Chebyshev, Taylor one-parameter, Taylor $\bar{n}$, Villeneuve $\bar{n}$, and those that allow side lobe envelope shaping. All distributions have constant phase.

A. Dolph–Chebyshev Arrays

The Dolph–Chebyshev pattern is conceptually simple, as it consists of a main pencil beam, plus side lobes of equal level. This was invented for a half-wave spaced broadside array by Dolph [2]. The oscillatory part of a Chebyshev polynomial is mapped onto the side lobes on one side of the pattern, while part of the $x > 1$ Chebyshev region is mapped onto half the main beam of the pattern. A direct mapping is not feasible as the main beam must be symmetric and have zero slope in the center. The number of zeros must also correspond, so an N element array is used with an $N - 1$ degree Chebyshev polynomial. The transformation from $T_{n-1}(x)$ to pattern $F(u)$ is given by $x = x_0 \cos(\pi u/2)$. The voltage SLR is given by

$$\text{SLR} = T_{N-1}(x_0). \tag{1}$$

The Dolph–Chebyshev pattern is given by

$$F(u) = T_{N-1}(x_0 \cos \pi u/2). \tag{2}$$

The excitation A_n of the nth element is obtained by writing the pattern with the array center as phase reference:

$$F(u) = \sum_{1}^{N} A_n \exp[j(2n - N - 1)\pi u/2]. \tag{3}$$

This is a finite Fourier series and the inverse gives the coefficients. These are easily calculated using formulas of Stegen [3]; his results are slightly different for odd and

0018–9219/92$03.00©1992 IEEE

even N, and may be used for spacings larger than half-wavelength.

A different mapping between the Chebyshev polynomial and the array pattern, which is valid for spacings less than half-wavelength has been developed, but only for N odd. An extensive discussion of these mappings and various formulas is given by Hansen [4].

For a given SLR, the Dolph–Chebyshev distribution yields the highest directivity and the narrowest beamwidth. However, the constant side lobe envelope violates one of Taylor's rules for obtaining a low-Q distribution. For large arrays with low side lobes, the distribution tends to be nonmonotonic, and may in fact have a peak at the end larger than the value in the center. Because of the high-Q of these distributions they are only occasionally used. Most often the Taylor distributions, which are quite robust, are used instead.

B. Taylor One-Parameter Distribution

In developing the one-parameter distribution, Taylor [5] started with the pattern from a uniformly excited aperture: $\sin \pi u/\pi u$. The far-out zeros are spaced by integers, and the side lobe envelope decays as $1/u$. Thus the only problem is the high level of close-in side lobes. These were reduced by shifting the close-in zeros to suitable values, where the zeros are now given by:

$$u = \sqrt{n^2 + B^2} \tag{4}$$

where B is the single parameter. The pattern is a modified sinc, and is written in two forms as:

$$F(u) = \frac{\sinh \pi\sqrt{B^2 - u^2}}{\pi\sqrt{B^2 - u^2}}, \qquad u \le B \tag{5}$$

$$F(u) = \frac{\sin \pi\sqrt{u^2 - B^2}}{\pi\sqrt{u^2 - B^2}}, \qquad u \ge B \tag{6}$$

A transition from the sinc pattern to the hyperbolic form occurs at $u = B$ on the side of the main beam. The SLR is that of the sinc times the beam peak value. This is, in dB,

$$\text{SLR} = 20 \log \frac{\sinh \pi B}{\pi B} + 13.26 \text{ dB} \tag{7}$$

The single parameter B controls all characteristics: side lobe level, beamwidth, efficiency, and beam efficiency (the fraction of power in the main beam, null-to-null). The aperture distribution is the inverse transform of the pattern, and is

$$g(p) = I_0\left(\pi B\sqrt{1 - p^2}\right) \tag{8}$$

where p is the distance from the center of the aperture to either end. I_0 is the modified Bessel function. The aperture (excitation) efficiency is given by

$$\eta = 2 \sinh^2 \pi B / \pi B \overline{I_0}(2\pi B) \tag{9}$$

where $\overline{I_0}$ is a tabulated integral [6], [7].

A typical Taylor one-parameter pattern is given in Fig. 9.22 of [4], and half of the symmetric aperture distribution is shown in Fig. 9.23 [4] for SLR's of 25, 30, and 40 dB. As expected, the patterns with lower side lobes have a lower pedestal at the end of the aperture. Table 1 gives the pertinent parameters, where u_3 is half the half-power beamwidth and η_b is the beam efficiency.

Table 1 Taylor One-Parameter Distribution Characteristics

SLR, dB	B	u_3 rad	η	η_b
13.26	0	0.4429	1	0.9028
20	0.7386	0.5119	0.9330	0.9820
25	1.0229	0.5580	0.8626	0.9950
30	1.2762	0.6002	0.8014	0.9986
35	1.5136	0.6391	0.7509	0.9996
40	1.7415	0.6752	0.7090	0.9999
45	1.9628	0.7091	0.6740	1.0
50	2.1793	0.7411	0.6451	1.0

C. Taylor $\overline{n}$ Distribution

A compromise between the Dolph–Chebyshev and the Taylor one-parameter distribution was developed by Taylor, and called the $\overline{n}$ distribution [1]. This offers a modest improvement in efficiency over the one-parameter distribution, by making the first few side lobes at equal level. Subsequent side lobes follow the $1/u$ envelope. The $\overline{n}$ distribution gives a narrower beamwidth and higher efficiency, without significantly degrading its robustness. The distribution is a modification of the continuous Taylor "ideal" line source [4], which is the equivalent of a Dolph–Chebyshev distribution, with a dilation factor used to modify the first $\overline{n}$ zeros. This factor is designed to produce a smooth transition from the few equal level side lobes to the $1/u$ envelope of side lobes. The pattern is given in two forms; a canonical finite product on $\overline{n} - 1$ zeros, or as a superposition of $\overline{n}$ sinc beams:

$$F(u) = \text{sinc } \pi u \sum_{n=1}^{\overline{n}-1} \frac{1 - u^2/z_n^2}{1 - u^2/n^2} = \sum_{n=-\overline{n}+1}^{\overline{n}-1} F(n, A, \overline{n}) \text{sinc } \pi(u + n) \tag{10}$$

The zeros are:

$$z_n = \pm\sigma\sqrt{A^2 + (n - 1/2)^2}, \qquad 1 \le n \le \overline{n}$$
$$z_n = \pm n, \qquad n \ge \overline{n}. \tag{11}$$

The coefficient in the equation is:

$$F(n, A, \overline{n}) = \frac{[(\overline{n} - 1)!]^2}{(\overline{n} - 1 + n)!\,(\overline{n} - 1 - n)!} \cdot \sum_{m=1}^{\overline{n}-1} \left(1 - n^2/z_m^2\right). \tag{12}$$

The dilation factor is:

$$\sigma = \overline{n}/\sqrt{A^2 + (\overline{n} - 1/2)^2} \tag{13}$$

Table 2 Taylor $\bar{n}$ Distribution Characteristics

SLR dB	A	u_3	$\bar{n} = 2$	4	6	8	10
				σ			
20	0.9528	0.4465	1.1255	1.1027	1.0749	1.0582	1.0474
25	1.1366	0.4890		1.0870	1.0683	1.0546	1.0452
30	1.3200	0.5284		1.0693	1.0608	1.0505	1.0426
35	1.5032	0.5653			1.0523	1.0459	1.0397
40	1.6865	0.6000			1.0430	1.0407	1.0364
45	1.8697	0.6328				1.0350	1.0328
50	2.0530	0.6639					1.0289

Here A is the single parameter. Strictly speaking this is a two-parameter distribution, but since $\bar{n}$ is so directly related to the characteristics of the pattern it is easy to choose. The aperture distribution is best expressed as a finite Fourier series:

$$g(p) = 1 + 2 \sum_{n=1}^{\bar{n}-1} F(n, A, \bar{n}) \cos n\pi p. \tag{14}$$

The excitation efficiency is simply:

$$\eta = \frac{1}{1 + 2 \sum_{1}^{\bar{n}-1} F^2(n, A, \bar{n})}. \tag{15}$$

A typical pattern is shown in Fig. 9.19 of [4]. Tables of aperture distribution and coefficients are given for SLR = 20(5)40 dB and $\bar{n} = 3(1)10$ by Hansen [8]. Fig. 9.20 of [4] shows half of symmetric aperture distributions for three combinations of SLR and $\bar{n}$. Table 2 gives typical parameters for this distribution.

There is an appropriate range of values for $\bar{n}$. A value too large will give results close to those of the Dolph–Chebyshev distribution: a nonmonotonic aperture distribution and large peaks at the ends. Too small a value of $\bar{n}$ will not allow the transition zone zeros to behave properly. The largest values of $\bar{n}$ that allow a monotonic distribution are given in Table 3, along with the values of $\bar{n}$ that produce maximum efficiency. It can be seen that the increase in efficiency over the monotonic case is very small, and hence the monotonic cases are almost always used.

The two Taylor distributions are widely used for linear and rectangular arrays due to their low-Q and good efficiency.

D. Villeneuve $\bar{n}$ Distributions

A discrete version of the Taylor $\bar{n}$ distribution, which is exact for both large and small arrays, was developed by Villeneuve [9]. He started with the Dolph–Chebyshev distribution, then the zeros past $\bar{n}$ were shifted to give a $1/u$ envelope. Just as the excitation coefficients for the Dolph–Chebyshev were slightly different for even and odd numbers of elements, the Villeneuve coefficients are similarly different. Although they are readily computed, the formulas are messy and are not repeated here; see [9], [10]. These excitation values are different for each size of array, so that for each new problem a new calculation must be made. This is in contrast to the sampling of the Taylor $\bar{n}$ distribution, where the simple formulas are good for all large arrays.

Table 3 Taylor $\bar{n}$ Efficiencies

SLR	Max η Values $\bar{n}$	η	$\bar{n}$	Monotonic $\bar{n}$ η
25	12	0.9252	5	0.9105
30	23	0.8787	7	0.8619
35	44	0.8326	9	0.8151
40	81	0.7899	11	0.7729

Of interest here is the relative efficiency of these finite $\bar{n}$ distributions. These have been calculated [10], and are shown in Table 4 for arrays with odd numbers of elements ranging from 5 to 41, and for SLR's of 25 to 40 dB. For comparison, Table 3 gives the Taylor $\bar{n}$ excitation efficiencies for comparable cases. It can be seen that arrays can be as small as 15 elements and have only a 3% loss in efficiency. Thus for small arrays, the exact Villeneuve $\bar{n}$ distribution should be used, while for roughly 20 or more elements, sampling of the Taylor $\bar{n}$ distribution is satisfactory.

E. Side Lobe Envelope Shaping

Control over the side lobe envelope of a pencil beam array is provided by adjusting individual side lobe heights, using techniques developed by Elliott [11]. Suppose that a cluster of side lobes is desired to have a low level while other side lobes can be higher. The side lobe envelopes on each side of the main beam need not be equal; the side lobe shaping applies to all side lobes. In this technique, after the desired pattern is sketched, a canonical pattern is selected so that the main beamwidth and the average side lobe level are roughly the same. The canonical pattern, which might be a Taylor one-parameter pattern, should be chosen to have the same number of pattern zeros. This pattern is then written as a product of zeros. Each zero of the desired pattern is assumed to be that of the canonical pattern plus a small shift. When higher order effects are discarded, the desired pattern can be written as the canonical pattern times a factor, which is one plus a sum over the zeros. This sum involves the pattern variable, the canonical pattern zeros, and the shifts in zeros that will produce the desired pattern. For low side lobes, the side lobe peak position is approximately halfway between the adjacent zeros. For each side lobe in the pattern, the side lobe peak position

Table 4 Villeneuve Max Monotonic $\overline{n}$

N	$\overline{n}$	SLB 25 dB	$\overline{n}$	SLR 30 dB	$\overline{n}$	SLR 35 dB	$\overline{n}$	SLR 40 dB
41	5	.9026	7	.8551	9	.8098	12	.7701
31	5	.9000	7	.8528	9	.8078	13	.7693
21	5	.8947	7	.8479	11	.8060	11	.7630
15	6	.8917	7	.8409	8	.7949	8	.7540
11	6	.8807	6	.8276	6	.7825	6	.7447
9	5	.8674	5	.8158	5	.7732	5	.7384
7	4	.8468	4	.7987	4	.7608	4	.7310
5	3	.8182	3	.7725	3	.7448		

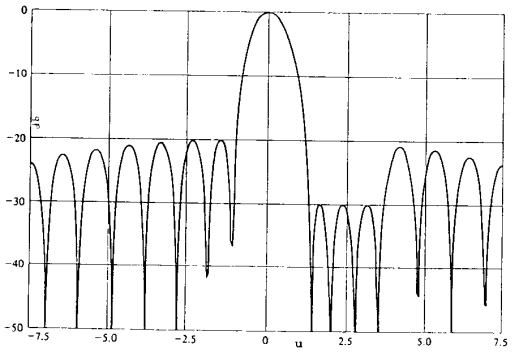

Fig. 1. Shaped side lobe pattern. (Courtesy Elliott.)

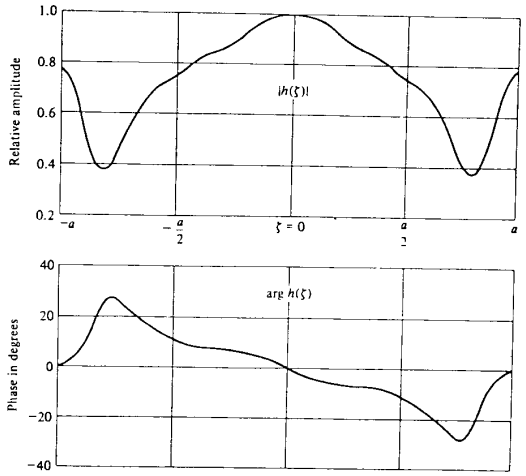

Fig. 2. Distribution for shaped side lobe pattern. (Courtesy Elliott.)

is inserted into the equation described above; this gives for each side lobe a relationship between the desired and canonical levels of that side lobe, and the various zeros. This then is a set of simultaneous equations, where the differences in side lobe heights are specified, and the zero shifts are the unknowns. These equations must be solved iteratively, using each resulting pattern in place of the canonical pattern of the previous step, until convergence is reached. A gradient scheme such as Newton–Raphson [12] gives a rapid way of finding the null shifts. Usually less than 10 iterations are needed.

The resulting pattern can be computed as a product on the zeros. To obtain the array excitation coefficients, the product form is multiplied out to obtain a sum, with the coefficients in the sum giving the array excitation values. An example of the results has been given by Elliott [13]. The objective was a Taylor $\overline{n} = 8$ distribution with 20 dB SLR, except for the three closest side lobes on the right side which should be at -30 dB. Figure 1 shows the resulting pattern, which required three iterations, while Fig. 2 shows the amplitude and phase of the resulting complex aperture distribution. This has proved to be a powerful technique for side lobe envelope shaping.

The method can also be used for the discretization of a continuous distribution when the number of array elements is too small to effectively realize the specified side lobe envelope. This is important because sampling is only applicable to longer arrays when very low side lobes are required. For this case the canonical starting pattern is just the sampled continuous distribution. Then the side lobe zeros are adjusted to produce the desired side lobe envelope.

III. A Pencil Beam from a Planar Array

Rectangular planar arrays are often designed using linear array distributions along the two principal axes. This gives patterns in the two principal planes that are linear array patterns, while the side lobes outside of these regions tend to be much lower, as they are the product of the side lobes of the two distributions. It is possible to synthesize a rectangular array distribution in which the side lobes in the principal planes are lower and those elsewhere are higher, such that the side lobe envelope surface is more slowly varying. However, these methods are not analytic but numeric, using such synthesis techniques as minimax or Simplex.

A. Hansen One-Parameter Circular Distribution

A symmetric distribution for circular disk arrays and apertures has been developed by Hansen [14]; this is analogous to the Taylor one-parameter linear distribution. Just as the latter was a modified sinc πu, this circular distribution is a modified $2J_1(\pi u)/\pi u$ pattern. The close-in zeros of the canonical pattern are shifted to produce the desired SLR. The pattern similarly has two forms, which

are:

$$F(u) = \frac{2I_1\left(\pi\sqrt{H^2 - u^2}\right)}{\pi\sqrt{H^2 - u^2}}, \qquad u \le H. \tag{16}$$

$$F(u) = \frac{2J_1\left(\pi\sqrt{u^2 - H^2}\right)}{\pi\sqrt{u^2 - H^2}}, \qquad u \ge H \tag{17}$$

The single parameter is H, and the J_1 and I_1 are the usual Bessel and modified Bessel functions of the first kind and order one. The SLR is given by:

$$\text{SLR} = 17.57 \text{ dB} + 20 \log \frac{2I_1(\pi H)}{\pi H}. \tag{18}$$

Table 5 gives parameters for this distribution. The aperture distribution is:

$$g(p) = I_0\left(\pi H\sqrt{1 - p^2}\right) \tag{19}$$

where I_0 is a modified Bessel function and the aperture extends to $p = \pm 1$. It is interesting that the circular and linear one-parameter patterns have the same aperture distribution, with only different constants. This is perhaps why this distribution was not developed along with the others by Taylor; he may have been expecting a more complex result. The excitation efficiency is obtained from a simple integration over the aperture:

$$\eta = \frac{2\left[\int_0^\pi g(p)p\,dp\right]^2}{\pi^2 \int_0^\pi g^2(p)p\,dp} = \frac{4I_1^2(\pi H)}{\pi^2 H^2[I_0^2(\pi H) - I_1^2(\pi H)]}. \tag{20}$$

Typical aperture distributions and patterns are given in [4, ch. 10].

Table 5 Hansen One-Parameter Distribution Characteristics

SLR dB	H	u_3 rad	η	η_b
17.57	0	0.5145	1	0.8378
25	0.8899	0.5869	0.8711	0.9745
30	1.1977	0.6304	0.7595	0.9930
35	1.4708	0.6701	0.6683	0.9981
40	1.7254	0.7070	0.5964	0.9994
45	1.9681	0.7413	0.5390	0.9998
50	2.2026	0.7737	0.4923	1.0000

B. Taylor $\overline{n}$ Circular Distribution

The Taylor $\overline{n}$ circular source distribution offers a modest improvement in efficiency and beamwidth over the Hansen one-parameter distribution, just as occurred for the linear distributions. Again the starting point is the uniform $2J_1(\pi u)/\pi u$ pattern. On each side of the main beam, $\overline{n}$ zeros are modified by moving them to produce the desired SLR [15]. Again a dilation factor σ is used to effect a smooth transition. The pattern is given by a finite product on the zeros:

$$F(u) = \frac{2J_1(\pi u)}{\pi u} \prod_{n=1}^{\overline{n}-1} \frac{1 - u^2/z_n^2}{1 - u^2/\mu_n^2}. \tag{21}$$

The pattern zeros are:

$$z_n = \pm\sigma\sqrt{A^2 + (n - 1/2)^2}, \qquad 1 \le n \le \overline{n} \tag{22}$$

and the dilation factor is:

$$\sigma = \frac{\overline{n}}{\sqrt{A^2 + (\overline{n} - 1/2)^2}}. \tag{23}$$

Here the μ_n are the zeros of $J_1(\pi u)$. The aperture distribution is given by a finite series:

$$g(p) = \frac{2}{\pi^2} \prod_{m=0}^{\overline{n}-1} \frac{F_m J_0(p\pi\mu_m)}{[J_o(\pi\mu_m)]^2}. \tag{24}$$

The coefficients are given in [4]. Extensive tables of these have been published [8], [16]. Table 6 gives the values of dilation factor and parameter A for various combinations of SLR and $\overline{n}$. The excitation efficiency is computed from integrals over the aperture as before; using Bessel function orthogonality results in a single series for the efficiency; see also [17]. Some efficiencies are shown in Table 7. Just as for the linear Taylor $\overline{n}$ distribution, there is a value of $\overline{n}$ that gives maximum efficiency. This value increases with SLR as may be observed.

For circular disk or octagonal arrays, these two distributions have found wide use, due to their high efficiency and low-Q.

IV. Difference Pattern Distributions

Difference patterns are useful in providing tracking for narrow beam antennas. Considered here are only those with a biphasal distribution, where one-half of the aperture is inphase, while the other half is 180 degrees out-of-phase. The simplest of these is the uniformly excited linear array, where the two halves of an array are fed, for example, through a 180-degree hybrid. This connection provides ports for the sum and difference patterns. The sum pattern is of course sinc u, while the difference pattern is:

$$F(u) = \sqrt{2}\,\frac{1 - \cos\pi u}{\pi u}. \tag{25}$$

The difference distribution is normalized so that the integral over the aperture distribution squared is unity; the peak value of the difference pattern is 1.0248 and the slope in the center is .7071. The first side lobe is -10.57 dB with respect to the peak. This is a simple distribution, but the side lobes are relatively high. Even worse are those of the maximum slope difference pattern [18], [19]. This distribution is triangular, a single sawtooth, with a peak (edge) value of 1.2247, using the same normalization. The pattern function is given by:

$$F(u) = \sqrt{6}\,\frac{\text{sinc } \pi u - \cos\pi u}{\pi u}. \tag{26}$$

Table 6 Taylor Circular $\bar{n}$ Distribution Characteristics

SLR dB	A	u_3	$\bar{n}=3$	4	5	6	7	8	9	10
						σ				
20	0.9528	0.4465	1.2104	1.1692	1.1398	1.1186	1.1028	1.0996	1.0910	1.0732
25	1.1366	0.4890	1.1792	1.1525	1.1296	1.1118	1.0979	1.0870	1.0782	1.0708
30	1.3200	0.5384	1.1455	1.1338	1.1180	1.1039	1.0923	1.0827	1.0749	1.0683
35	1.5032	0.5653		1.1134	1.1050	1.0951	1.0859	1.0779	1.0711	1.0653
40	1.6865	0.6000		1.0916	1.0910	1.0854	1.0789	1.0726	1.0560	1.0620

Table 7 Taylor Circular $\bar{n}$ Efficiency

SLR dB	$\bar{n}=4$	5	6	8	10
20	0.9723	0.9356	0.8808	0.7506	0.6238
35	0.9324	0.9404	0.9379	0.9064	0.8536
30	0.8482	0.8623	0.8735	0.8838	0.8804
35	0.7708	0.7779	0.7880	0.8048	0.8153
40	0.7056	0.7063	0.7119	0.7252	0.7365

The beam peak is a little closer to the center of the pattern; the slope is .81650. However the first side lobe is only −8.28 dB, which makes this pattern unattractive.

The formula used to compute excitation efficiency for equiphase apertures [20] must be modified for difference pattern distributions to include the pattern peak location u_0:

$$\eta = \frac{\left[\int g(p)\exp j\pi p u_0\, dp\right]^2}{2\int g^2(p)\, dp}. \tag{27}$$

Since difference patterns with high side lobes cause poor tracking due to interference, clutter, etc., it was to be expected that the zero shifting principles of pattern adjustment would be applied here. This was done by Bayliss [21], who produced a difference pattern analogous to the Taylor $\bar{n}$ pattern. A starting point is the Taylor "ideal" line source sum pattern (see Section II-C), which is differentiated to obtain a difference pattern. When this pattern is examined it is seen that the side lobes are of irregular levels, and the envelope is nonmonotonic. An iterative procedure was used to adjust these zeros to yield equal level side lobes. It was necessary to adjust only four, but these four zeros depend upon the SLR. Bayliss gives results in terms of fourth order polynomials in SLR. The four zeros, the parameter A, and u_0 which is the difference peak location, are given in Table 8. These zeros are applicable for both linear arrays and for circular planar arrays. The remainder of the zeros are the same as for the linear Taylor $\bar{n}$ case. The pattern is given by a ratio of finite products, which replaces the first $\bar{n}$ zeros of $\cos \pi u$ by the modified set, or by a finite sum:

$$F(u) = \sum_{n=0}^{\bar{n}-1} B_n \frac{(-1)^n u \cos \pi u}{(n+1/2)^2 - u^2}. \tag{28}$$

The zeros z_n are given in the table for $n = 1-4$, and for $n > 4$ are:

$$z_n = \pm\sqrt{A^2 + n^2}. \tag{29}$$

The dilation factor is given by:

$$\sigma = (\bar{n} + 1/2)/z_{\bar{n}}. \tag{30}$$

Figure 3 gives a typical Bayliss pattern, which is for a 25-dB SLR and $\bar{n} = 5$. The aperture distribution is given by:

$$g(p) = \sum_{n=0}^{\bar{n}-1} B_n \sin \pi/(n+1/2)p \tag{31}$$

where the coefficient is:

$$B_m = -(-1)^m (m-1/2)^2 \cdot \frac{\prod_{n=1}^{\bar{n}-1}\left\{1 - [(m+1/2)/\sigma z_n]^2\right\}}{\prod_{\substack{n=0 \\ n\neq m}}^{\bar{n}-1}\left\{1 - [(m+1/2)/(n+1/2)]^2\right\}}. \tag{32}$$

The amplitude of the aperture distribution is shown for the same case in Fig. 4. The excitation efficiency, defined here as the directivity at one difference peak u_0 divided by that of a uniformly excited sum line source, is given by:[1]

$$\eta = \frac{2u_0^2 \cos^2 \pi u_0 \sum_{n=0}^{\bar{n}-1} (-1)^n B_n \Big/ \left[u_0^2 - (n+1/2)^2\right]^2}{\sum_{n=0}^{\bar{n}-1} B_n^2}. \tag{33}$$

Finally the slope at the center is given by:

$$S = (2/\pi)\sum_{n=0}^{\bar{n}-1} (-1)^n B_n/(n+1/2)^2. \tag{34}$$

Table 9 gives the efficiency compared to a sum pattern, and the normalized slope, where that of the maximum slope pattern is unity.

A Bayliss distribution was also developed for symmetric circular apertures, analogous to the circular Taylor $\bar{n}$ pattern. The development parallels that for the circular Taylor case, with the adjusted first four zeros mentioned previously used here also. For details, see [21], [22].

Since the array distributions that produce good difference pattern side lobes are quite different from those that produce good sum pattern side lobes, ways have been developed for independently optimizing both distributions. Two of these methods will now be briefly discussed. The tandem feed was invented by Kinsey [23]. In its best (symmetric) form,

[1] Unpublished calculations by R. C. Hansen.

Table 8 Bayliss Line Source Parameters

SLR, dB	15	20	25	30	35	40
A	1.00790	1.22472	1.43546	1.64126	1.84308	2.04154
z_1	1.51240	1.69626	1.88266	2.07086	2.26025	2.45039
z_2	2.25610	2.36980	2.49432	2.62754	2.76748	2.91234
z_3	3.16932	3.24729	3.33506	3.43144	3.53521	3.64518
z_4	4.12639	4.18544	4.25273	4.32738	4.40934	4.49734
u_0	0.66291	0.71194	0.75693	0.79884	0.83847	0.87649

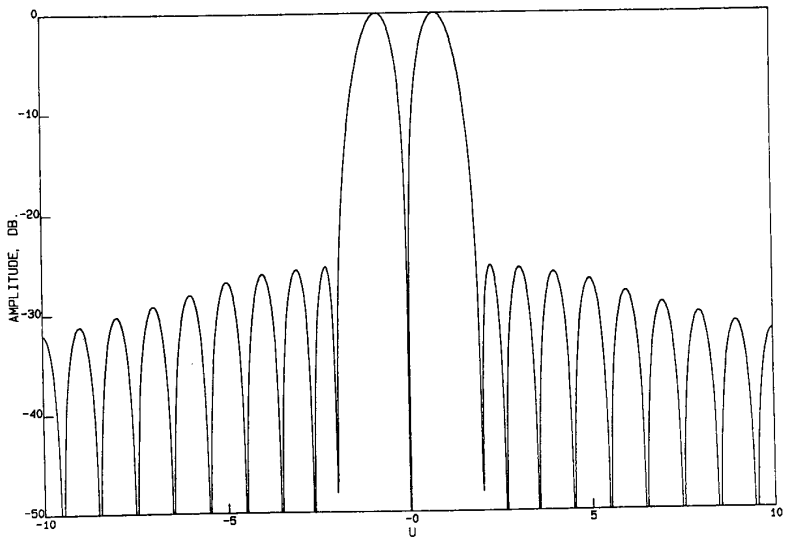

Fig. 3. Bayliss $\overline{n} = 5$ Pattern, SLR = 25 dB.

Table 9 Bayliss Efficiency and Pattern Slope

SLR dB	$\overline{n}$	Efficiency	Normalized Slope
15	4	0.5959	0.9567
20	4	0.5846	0.8974
25	5	0.5633	0.8427
30	6	0.5393	0.7912
35	7	0.5162	0.7448
40	8	0.4951	0.7037

it consists of a ladder network, with a directional coupler at the end of each rung. The inboard arms of the couplers are connected along the rungs, while the outboard arms on one side are connected to the linear array elements, with the outboard arms on the other side terminated in loads. At the center of each of the ladder rails is located a hybrid junction, with the outputs of these connected to give the sum and difference ports. The rail of couplers adjacent to the array provides the sum excitation; both rails of couplers provide the difference excitation. This arrangement, although complex, gives excellent control of both sum and difference patterns; see [24], [25].

A simpler scheme divides a linear array symmetrically into subarrays, which need not be of equal length. Symmetric pairs of subarrays are connected to a hybrid junction. A stair-step approximation to the desired sum pattern distribution is provided by connecting the sum port of the hybrids to suitable power divider. Similarly a different power divider provides a stair-step approximation to the desired difference pattern distribution [26]. Obviously as more subarrays of smaller size are used, the stair-step approximations become better, and the resulting patterns are closer to those desired. The same procedure has been applied to planar arrays by Josefsson and others [27]. Here the array is divided into subarrays, usually quadrantly symmetric. Again the number of elements, and the shape in each subarray, is often different. Symmetric pairs are then connected to hybrid junctions; these hybrids are then connected to the sum and the two difference feed networks, again to provide a stair-step approximation to the three desired distributions. Excellent results have been obtained even with only a small number of subarrays per quadrant. This scheme is especially attractive with printed circuit antennas, as this implementation fits well with realizing the feed networks in stripline.

V. A Shaped Beam from a Linear Array

For many applications a pencil beam is not appropriate, as for example, in radar where a cosecant type beam

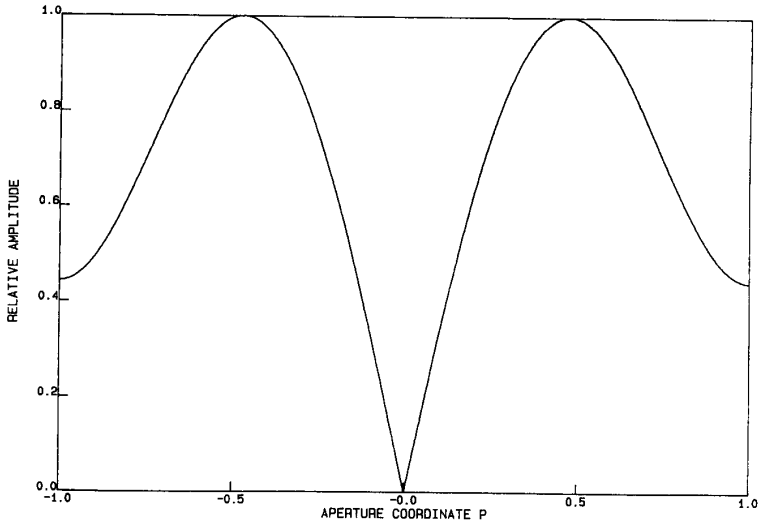

Fig. 4. Bayliss $\bar{n} = 5$ Distribution, SLR = 25 dB.

is often used. This section discusses the two principal methods used for synthesizing shaped beams from a linear array: the classical Woodward–Lawson, and the newer Orchard–Elliott methods.

A. Woodward–Lawson Synthesis

The Woodward–Lawson synthesis [28] utilizes a set of multiple beams from an array or aperture. These are simple sinc beams of the form:

$$E_n = \operatorname{sinc} \pi\left[\frac{L}{\lambda}\sin\theta - n\right]. \tag{35}$$

This equation is for a continuous aperture; the equivalent form of $\sin Nx/N \sin x$ is used for an array. These sinc beams are spaced apart from each other such that at an angle where one beam has a peak, all of the other beams have nulls. Thus the Woodward–Lawson synthesis is simply a matter of adding a series of these beams with each weighted equal to the value of the desired pattern at that sampling point. The aperture or array distribution is then the sum of constant amplitudes, each weighted by the appropriate factor, and linear phases, each having a tilt appropriate to the beam position. The result for a csc θ pattern, for example, has a symmetric amplitude distribution with a large peak in the center (representing the largest beam at the start of the cosecant pattern), with the rest of the distribution being oscillatory and lower. The phase is roughly linear with oscillations, ranging from $-\pi$ at one end to π at the other end, with skew symmetry about the center. This synthesis technique is easy to understand and easy to use, and is natural for arrays that inherently involve multiple beams. An example is the Rotman lens, where each beam port may simply be weighted and summed to generate a shaped beam pattern [29]–[33]. However the Woodward–Lawson technique has a serious intrinsic limitation in that the pattern zeros occur in pairs. This means that there are only half as many adjustments available as there could be for a given number of elements in an array. The practical result is that in the shaped pattern region, the number of ripples is half what it could be, and thus the ripples tend to be larger. A less critical difficulty with this method is that of controlling the side lobes outside the shaped beam region. Fortunately with modern computers and the techniques of zero placement previously discussed, better synthesis techniques are available and one will be discussed next.

B. Orchard–Elliott Synthesis

The Orchard–Elliott synthesis is quite similar to that used in Section II-E for side lobe envelope shaping, except that here a power pattern is synthesized. To understand this, the pattern is written in terms of the previously used variable u and then expanded into a product on the zeros of the array polynomial with variable $w = \exp ju$. Next each zero is expressed in exponential form: $w_n = \exp(a_n + jb_n)$. One of the roots is anchored at $-1 + j0$. The power pattern in dB is then given by a sum over the roots:

$$P(u) = \sum_{n=1}^{N-1} 10\log\left[1 - 2\exp a_n \cos(u - b_n) + e^{2a_n}\right] + 10\log 2(1 + \cos u) + C. \tag{36}$$

The constant C is used to set the level of the pattern. If the specified pattern is $S(u)$, a total differential of the difference between the specified pattern and the pattern expressed above gives:

$$d(P - S) = \sum_{n=1}^{N-1}\left[\frac{\partial p}{\partial a_n}da_n + \frac{\partial p}{\partial b_n}db_n\right]. \tag{37}$$

When this equation is implemented at a sequence of u values at the ripple peaks and troughs in the shaped portion of the pattern, and at the side lobe peaks in

the side lobe portion, a set of simultaneous equations results. These equations can be solved iteratively using the Newton–Raphson technique described earlier to obtain the shifts in the zeros. At each step in the iterative process, the new locations of peaks, troughs and side lobes must be determined. Usually less than a dozen iterations are sufficient. When the final complex roots are obtained, via the coefficients a_n and b_n, they are inserted into the pattern equation to obtain the final pattern [34], [35]. The shaped beam region is formed by some of the nulls located off the unit circle. It is interesting to note that essentially the same patterns can result from pairs of these nulls either outside or inside the unit circle, thus giving four design option cases. Elliott has observed that the array distributions that accompany these four cases are generally quite different, so that the designer should make adjustments during the iterative process to obtain in turn each of the four cases, so that the best aperture distribution in terms of array realization may be used. This then is another powerful pattern synthesis technique using the physical principles of adjusting zeros in the array pattern polynomial.

VI. Superdirective Arrays

A. Arrays

Superdirectivity, formerly called supergain, exists when an antenna exhibits directivity greater than normal; normal directivity occurs for a broadside array when the elements are spaced half-wavelength apart, and for an endfire array with quarter-wavelength spacing. These arrays were established conceptually at least as early as 1922 by Oseen (see [36]). The major investigative work occurred in the 1950's, with a now almost complete understanding of the phenomenon. An extensive list of references is given in [36]. Superdirective arrays possess fundamental limitations, as the Q increases rapidly as directivity increases above normal. Since bandwidth for narrow band matched systems is approximately $2/Q$, these arrays have narrow bandwidth. Another limitation occurs because the input resistance of the elements decreases, making impedance matching difficult. Further, the allowable tolerances on the excitation of the array elements decrease rapidly with increase in directivity.

A superdirective array may be designed to have maximum directivity, to have maximum directivity subject to a side lobe level constraint (Dolph–Chebyshev design), or maximum directivity subject to a constraint on Q or tolerances. To understand the capabilities and limitations of superdirective arrays, maximum directivity without constraints will be used. In addition, since maximum directivity occurs for an endfire array [37], only these are considered here. Ring arrays and broadside linear arrays are less effective. The maximum directivity array excitation coefficients are, in general, complex at angles off broadside. The directivity for a linear endfire array of dipoles of length ℓ can be written in terms of mutual resistances:

$$G = \frac{120|\sum A_n V_n^*|^2 \tan^2 \pi l/\lambda}{\sum\sum A_n A_m R_{nm}}. \tag{38}$$

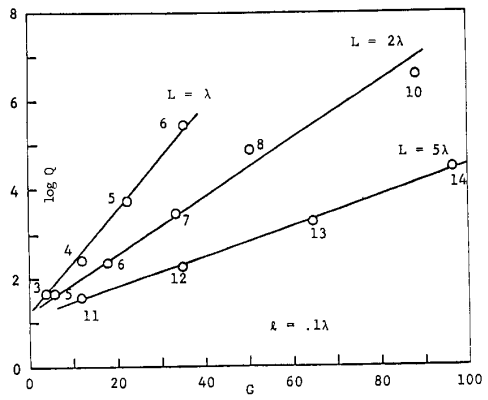

Fig. 5. Q of endfire arrays of parallel dipoles.

For dipole or slot elements the resistances are provided by a Sine and Cosine Integral subroutine [38], while for isotropic elements the virtual mutual resistance of 120 sinc kd is used. The directivity is maximized by a Lagrangian multiplier scheme, which results in a set of complex simultaneous equations. These are solved for the array excitation coefficients, which are then substituted into the directivity expression. The Q is given by:

$$Q = \frac{120 \sum A_n A_n^*}{\sum\sum A_n A_m^* R_{nm}}. \tag{39}$$

For arrays of significant superdirectivity, the formulas involve subtracting large numbers, especially for Q. Thus it is necessary to use double precision in the calculation of the mutual resistances, and hence for the Sine and Cosine Integrals. A Chebyshev economized series expansion developed by Luke [39] is used to construct a double precision subroutine. Figure 5 gives log Q versus directivity G for arrays of length one, two, and five wavelengths; parallel dipoles of .1 wavelength are used [40]. It is interesting that the variation of log Q with directivity is almost linear for a given length of array, and that the slope changes markedly with array length. Longer arrays are more robust. The conclusion is that only modest directivity increases, usually less than 3 dB, can be utilized, as larger increases incur high Q's.

B. Superconducting Arrays

With the advent of high T_c materials, no discussion of superdirective arrays would be complete without mentioning the possibilities offered by these new superconductors. For superdirective arrays, the materials might be used in the antenna, or in the matching network. Figure 6 shows radiation resistance of the center element of a number of arrays versus Q. It can be noted that for radiation resistance as low as .1 ohms, the Q is already two thousand. This would give an antenna bandwidth of .1%, which is generally not useful. Typical loss resistances are much less than .1 ohm; for superdirective arrays where conduction loss plays a significant role, the Q's are generally many

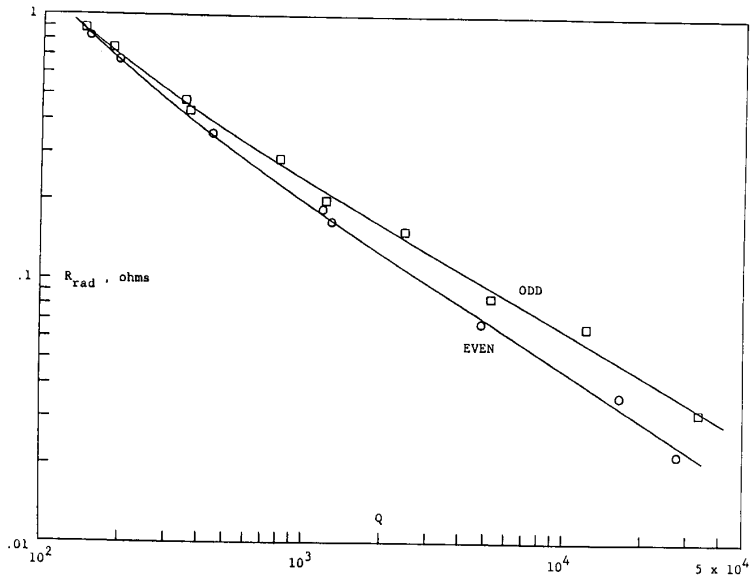

Fig. 6. Q versus center element resistance for endfire arrays.

thousands, and the array is impractical [41]. Consequently superconductors are not needed for the antenna itself.

However, for the matching network the outcome is completely different. All matching networks involve one or more resonant circuits, either lumped or distributed, and they may be represented roughly by a single lossy transmission line match. For this case, a matching line with a matched loss of L has a net loss with a mismatch $VSWR$ of V, of:

$$L_{\text{net}} = \frac{(V+1)^2L^2 - (V-1)^2}{4VL}. \tag{40}$$

To show how serious is this increase of loss, a 1 ohm radiation resistance matched to 50 ohms gives $V = 50$, while a reactance of 10 000 with this resistance gives $V = 20\,000$. From these numbers it can be seen that even very small losses in a matching network rapidly magnify to significant losses. To give an example, Khamas, *et al.* [42] measured UHF dipoles of copper and 1-2-3 superconducting material, both with matching stubs. The dipole efficiency was near 100%, while the matching network loss was of the order of 12 dB for the copper case. Thus the loss is essentially in the matching circuit.

The conclusions for superdirective arrays are as follows. Arrays of modest superdirectivity are useful, and they can be synthesized either for maximum directivity or with a limit on Q. Superconducting materials are extremely attractive for use in the matching network, but are not needed in the antenna itself.

REFERENCES

[1] T. T. Taylor, "Design of line-source antennas for narrow beamwidth and low side lobes," *Trans. IRE*, vol. AP-3, pp. 16–28, 1955.

[2] C. L. Dolph, "A current distribution for broadside arrays which optimizes the relationship between beam width and side-lobe level," *Proc. IRE*, vol. 34, pp. 335–348, June 1946.

[3] R. J. Stegen, "Excitation coefficients and beamwidths of Tschebyscheff arrays," *Proc. IRE*, vol. 41, pp. 1671–1674, Nov. 1953.

[4] R. C. Hansen, Array chapters in *Handbook of Antenna Design, Vol. 2*, A. W. Rudge, *et al.* Eds. IEE/Peregrinus, 1983.

[5] T. T. Taylor, "One-parameter family of line sources producing modified sin $\pi u/\pi u$ patterns," Hughes Aircraft Co., Culver City, CA, Rep. TM 324, 1953.

[6] M. Rothman, "Table of $\int I_0(x)\,dx$ for 0(0.1)20(1)25," *Quart. J. Mech. Appl. Math.*, vol. 2, pp. 212–217, 1949.

[7] M. Abramowitz and L. Stegun, *Handbook of Mathematical Functions*, National Bureau of Standards, 1970.

[8] R. C. Hansen, *Microwave Scanning Antennas, Vol. 1*. New York: Academic Press, 1964, ch. 1; Peninsula Publ., 1985.

[9] A. T. Villeneuve, "Taylor patterns for discrete arrays," *IEEE Trans. Antennas Propagat.*, vol. AP-32, pp. 1089–1093, Oct. 1984.

[10] R. C. Hansen, "Aperture efficiency of Villeneuve $\bar{n}$ arrays," *IEEE Trans. Antennas Propagat.*, vol. AP-33, pp. 666–669, June 1985.

[11] R. S. Elliott, "Design of line-source antennas for sum patterns with side lobes of individually arbitrary heights," *IEEE Trans. Antennas Propagat.*, vol. AP-24, pp. 76–83, Jan. 1976.

[12] P. A. Stark, *Introduction to Numerical Methods*. New York: MacMillan, 1970.

[13] R. S. Elliott, "On discretizing continuous aperture distributions," *IEEE Trans. Antennas Propagat.*, vol. AP-25, pp. 617–621, Sept. 1977.

[14] R. C. Hansen, "A one-parameter circular aperture distribution with narrow beamwidth and low side lobes," *IEEE Trans. Antennas Propagat.*, vol. AP-24, pp. 477–480, July 1976.

[15] T. T. Taylor, "Design of circular apertures for narrow beamwidths and low side lobes," *Trans. IRE*, vol. AP-8, Jan. 1960, pp. 17–22.

[16] R. C. Hansen, "Tables of Taylor distributions for circular aperture antennas," *Trans. IRE*, vol. AP-8, pp. 23–26, Jan. 1960.

[17] R. C. Rudduck *et al*, "Directive gain of circular Taylor patterns," *Radio Sci.*, vol. 6, pp. 1117–1121, Dec. 1971.

[18] E. J. Powers, "Utilization of the Lambda functions in the analysis and synthesis of monopulse antenna difference patterns," *IEEE Trans. Antennas Propagat.*, vol. AP-15, pp. 771–777, Nov. 1967.

[19] G. M. Kirkpatrick, "Aperture illuminations for radar angle-of-arrival measurements," *Trans. IRE*, vol. ANE-9, pp. 20–27, Sept. 1953.

[20] H. T. Friis and W. D. Lewis, "Radar antennas," *BSTJ*, vol. 26, pp. 219–317, 1947.

[21] E. T. Bayliss, "Design of monopulse antenna difference patterns with low side lobes," *BSTJ*, vol. 47, pp. 623–650, May-June 1968.

[22] R. S. Elliott, *Antenna Theory and Design*. Englewood Cliffs, NJ: Prentice-Hall, 1981.

[23] R. R. Kinsey, "Tandem series-feed system for array antennas," Patent 3509577, Apr. 1970.
[24] A. R. Lopez, "Monopulse networks for series feeding an array antenna," *IEEE Trans. Antennas Propagat.*, vol. AP-16, pp. 436–440, July 1986.
[25] W. R. Jones and E. C. DuFort, "On the design of optimum dual-series feed networks," *IEEE Trans. Microwave Theory Tech.*, vol. MTT-19, pp. 451–458, May 1971.
[26] R. R. Kinsey, "The AN/TPS-59 antenna row-board design," *IEEE APS Symp. Dig.*, 1974, pp. 413–416.
[27] L. Josefsson, L. Moeschlin and V. Sohtell, "A monopulse flat plate antenna for missile seeker," presented at the Military Electronics Defense Expo, Weisbaden, West Germany, Sept. 1977.
[28] P. M. Woodward and J. D. Lawson, "The theoretical precision with which an arbitrary radiation pattern may be obtained from a source of a finite size," *JIEE*, vol. 95, pp. 363–370, pt. III, 1948.
[29] W. Rotman and R. F. Turner, "Wide-angle microwave lens for line source applications," *IEEE Trans. Antennas Propagat.*, vol. AP-11, pp. 623–632, Nov. 1963.
[30] M. S. Smith, "Design considerations for Ruze and Rotman lenses," *Radio and Electronic Engineer*, vol. 52, pp. 181–197, Apr. 1982.
[31] M. J. Maybell, "Printed Rotman lens-fed array having wide bandwidth, low side lobes, constant beamwidth and synthesized radiation pattern," *IEEE APS Symp. Dig.*, 1983, pp. 373–376.
[32] D. H. Archer, "Lens-fed multiple beam arrays," *Microwave J.*, vol. 27, pp. 171–195, Sept. 1984.
[33] D. L. Johnson *et al.*, "Octave bandwidth, −35 dB side lobe single offset pillbox reflector using a Rotman lens and array as a primary feed," *IEEE APS Symp. Dig.*, 1987, pp. 195–198.
[34] H. J. Orchard *et al.*, "Optimizing the synthesis of shaped beam antenna patterns," *Proc. IEE*, vol. 132H, pp. 63–68, Feb. 1985.
[35] Y. U. Kim and R. S. Elliott, "Shaped-pattern synthesis using pure real distributions," *IEEE Trans. Antennas Propagat.*, vol. AP-36, pp. 1645–1649, Nov. 1988.
[36] R. C. Hansen, "Fundamental limitations in antennas," *Proc. IEEE*, vol. 69, pp. 170–182, Feb. 1981.
[37] Y. T. Lo *et al.*, "Optimization of directivity and signal-to-noise ratio of an arbitrary antenna array," *Proc. IEEE*, vol. 54, pp. 1033–1045, Aug. 1966.
[38] R. C. Hansen, "Formulation of echelon dipole mutual impedance for computer," *IEEE Trans. Antennas Propagat.*, vol. AP-20, pp. 780–781, Nov. 1972.
[39] Y. L. Luke, *Mathematical Functions and Their Approximations*. New York: Academic Press, 1975.
[40] R. C. Hansen, "Some new calculations on antenna superdirectivity," *Proc. IEEE*, vol. 69, pp. 1365–1366, Oct. 1981.
[41] ——, "Superconducting antennas," *IEEE Trans. Aerosp. Electron. Syst.*, vol. 26, pp. 345–355, Mar. 1990.
[42] S. K. Khamas *et al.*, "A high-T_c superconducting short dipole antenna," *Electron. Lett.*, vol. 24, pp. 460–461, Apr. 1988.

R. C. Hansen (Life Fellow, IEEE) received the B.S.E.E. degree from the Missouri School of Mines and the Ph.D. degree from the University of Illinois, Urbana.

From 1949 to 1955 he worked in the Antenna Laboratory of the University of Illinois on ferrite loops, streamlined airborne antennas, and DF and homing systems. In 1960 he became a senior staff member in the Telecommunications Laboratory of STL, Inc., engaged in communication satellite telemetry, tracking, and command. Earlier he was section head in the Microwave Laboratory of Hughes Aircraft Co., where he worked on surface wave antennas, slot arrays, near-fields and radio power transfer, electronic scanning and steerable arrays, and dynamic antennas. From 1964 to 1966, he formed and was the director of the Test Mission Analysis Office and was responsible for computer programs for the planning and control of classified Air Force Satellites. Prior to this, as Associate Director of Satellite Control, he was responsible for converting the Air Force satellite control network into a real-time computer-to-computer network. From 1966 to 1967 he was Operations Group Director of the Manned Orbiting Laboratory Systems Engineering Office of the Aerospace Corp. and was responsible for flight crew training, simulator, the software system for mission profiles, and mission control center equipment and displays. Since 1971 he has been a consulting engineer for antennas and systems related problems.

Dr. Hansen has written over 100 papers on electromagnetics, has been an Associate Editor of *Microwave Journal* since 1960, was the Associate Editor of *Radio Science* from 1967 to 1969, was the Associate Editor of *Microwave Engineer's Handbook* in 1971, was the Editor of *Microwave Scanning Antennas, Vol. I* in 1964 and of *Vols. II and III* in 1966, was the Editor of *Significant Phased Array Papers* in 1973, of *Geometric Theory of Diffraction* in 1981, and of *Moment Methods in Antennas and Scattering* in 1990. Many of his professional activities include: Chairman of U.S. Commission VI of URSI from 1967 to 1969, Chairman of the 1958 WESCON Technical Program Committee, Chairman of APS from 1963 to 1964 and in 1980, Chairman of Standards Subcommittee 2.5 which revised *Methods of Testing Antennas*, Editor of *APS Newsletter* from 1961 to 1963, member of APS AdCom from 1959 to 1974, member of the IEEE Publications Board in 1972 and 1974, and the Director IEEE in 1975. He is a fellow of the IEE, is a registered Professional Engineer in California and England, and is a member of the American Physical Society, Tau Beta Pi, Sigma Xi, Eta Kappa Nu, and Phi Kappa Phi. He was awarded an honorary Doctor of Engineering degree by the University of Missouri-Rolla in 1975. The University of Illinois Electrical Engineering Department gave him a Distinguished Alumnus award in 1981, and the College of Engineering awarded a Distinguished Alumnus Service Medal in 1986. He received the Barry Carlton best paper prize from the IEEE AES Society for 1990.